electronics

MDPI

Article

Combining Distributed Consensus with Robust H_∞-Control for Satellite Formation Flying

Julian Scharnagl [1],*, Florian Kempf [2] and Klaus Schilling [2]

[1] Zentrum für Telematik e.V., Magdalene-Schoch-Straße 5, 97074 Würzburg, Germany
[2] Department of Computer Science, Julius-Maximilians-Universität Würzburg, Am Hubland, 97074 Würzburg, Germany; kempf@informatik.uni-wuerzburg.de (F.K.); schi@informatik.uni-wuerzburg.de (K.S.)
* Correspondence: julian.scharnagl@telematik-zentrum.de; Tel.: +49-931-6156-3336

Received: 20 January 2019; Accepted: 10 March 2019; Published: 13 March 2019

Abstract: Control methods that guarantee stability in the presence of uncertainties are mandatory in space applications. Further, distributed control approaches are beneficial in terms of scalability and to achieve common goals, especially in multi-agent setups like formation control. This paper presents a combination of robust H_∞ control and distributed control using the consensus approach by deriving a distributed consensus-based generalized plant description that can be used in H_∞ synthesis. Special focus was set towards space applications, namely satellite formation flying. The presented results show the applicability of the developed distributed robust control method to a simple, though realistic space scenario, namely a spaceborne distributed telescope. By using this approach, an arbitrary number of satellites/agents can be controlled towards an arbitrary formation geometry. Because of the combination with robust H_∞ control, the presented method satisfies the high stability and robustness demands as found e.g., in space applications.

Keywords: distributed control; robust control; consensus; H_∞; satellite formation flying; formation control

1. Introduction

The satellite formation flying (SFF) is an evolving research area leading to new applications in space. Various attempts have been undertaken to achieve distributed mission architectures reducing costs, development time, increasing failure safety and expanding possibilities for further mission concepts. Contributing to the improvement of telecommunications and Earth and deep space observation missions, the distribution of satellite systems flying in proximity using 3D formations has yet to prove itself valuable in real world applications. One of the main challenges in SFF is position control. Especially for formations with higher numbers of satellites, scalability and robustness plays a significant role which precludes hierarchical approaches and demands decentralized or distributed methods.

So far, there have been different SFF missions demonstrating accurate stationkeeping of satellites like the Magnetospheric Multiscale Mission (MMS) mission from NASA [1] or autonomous acquisition and maintenance of a force free formation within the CanX-4 and 5 mission. This mission from University of Toronto was the first research mission to form a projected circular orbit (PCO) formation, specifically for two satellites, at about 50 m and 100 m semi-major axis of the PCO ellipse [2]. The upcoming NetSat mission (to be launched 2019) aims at developing and demonstrating efficient guidance and control of dynamically evolving formation topologies in a distributed way. The mission consists of four identical spacecraft equipped with 8.0 µN low thrust propulsion and a mass of approximately 1.3 kg [3].

Different control strategies have been proposed for formation control in these missions and also in recent literature. For example linear quadratic regulator (LQR) was used in the CanX-4 and 5 mission [2]. model predictive control (MPC) has been proposed by the authors for continuous low thrust formation flying applications especially in the frame of the NetSat mission [4] as well as plant-inversion based control using a reference governor [5]. Also robust control based on H_∞ synthesis was applied in the rendezvous phase of ESA's automated transfer vehicle (ATV) [6]. In addition, different robust control approaches have been discussed for SFF, e.g., Franzini and Innocenti [7] generalized H_∞ control for nonlinear systems using a state-dependent Riccati equation for relative motion of two satellites including perturbations (J2, atmospheric drag).

Beyond SFF, the topic of formation control is also of major interest in many other applications, e.g., Saska et al. [8] show a method for controlling formations of autonomous vehicles in order to reach a desired target region based on virtual leaders whose control inputs are obtained using MPC. Especially for applications with robustness requirements and partly unknown system parameters adaptive iterative learning reliable control (AILRC) is of interest (cf. e.g., [9]). Beyond that, Haidegger et al. [10] present a robust cascade control approach for telerobots in space medicine which is designed with focus on the high robustness requirements in space.

Robust control methods can guarantee stability within a specific range of uncertainties, which is of special interest for space applications because of high safety demands due to the fact that single errors can lead to the failure of a whole mission (cf. [11,12]). Distributed control methods provide scalability and the possibility to control a formation towards a joined goal (cf. [13]). Both aspects are beneficial for SFF and crucial for certain (future) space applications like distributed large-scale spaceborne telescopes.

There have been different approaches on combining robust and distributed control methods (cf. [14,15]). Massioni et al. [16] present a decomposition-based approach to design a distributed controller that guarantees H_∞ performance for SFF. Without focusing on space applications, Li et al. [17] designed a two-step algorithm that guarantees H_∞ performance for multi-agent systems using the consensus method. In addition, Xue et al. [18], Amini et al. [19] and Li and Chen [20] are among the publications within this field that influenced this work. This research activity combines distributed control in the sense of the consensus method with robust control in the sense of H_∞ synthesis for the application of SFF.

2. Materials and Methods

This chapter provides the foundations of this research work as well as the theoretical developments. First, the coordinate system and dynamic model is introduced. Second, required fundamentals in graph theory and control are presented. Third, distributed and robust control is introduced and the required definitions are given. Last, the acquired distributed consensus method is combined with robust H_∞-control.

2.1. Coordinate System

The coordinate system used in this paper is the local-vertical, local-horizontal (LVLH) coordinate system as defined by European Space Agency (ESA) and the International Space Station (ISS) program [21] as shown in Figure 1. (There are multiple definitions of LVLH with differently labeled axes.)

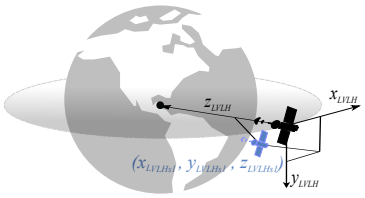

Figure 1. Local-vertical, local horizontal (LVLH) coordinate system with x-axis tangential to flight direction along the satellite's orbit, z-axis towards Earth center and y axis completing the right-handed coordinate system.

2.2. Linear Model of Satellite Dynamics

To develop and implement a controller a model, describing the behaviour of the specific system is necessary. In many SFF applications the Hill's equations [22] can be used as a good approximation providing a linearized set of equations of motion. Thus they are chosen as the model. In general, they describe the relative motion of a chaser with respect to a leader spacecraft as differential equations. Being an approximation, the Hill's equations show errors with respect to actual satellite behaviour. Depending on individual accuracy requirements they should only be applied within close range of up to few tens of kilometers and nearly circular orbits with small eccentricities in the order of $\leq 10^{-3}$. They are given in LVLH as

$$\ddot{x} - 2\,\omega\,\dot{z} = \frac{1}{m_c} F_x \tag{1a}$$

$$\ddot{y} + \omega^2\, y = \frac{1}{m_c} F_y \tag{1b}$$

$$\ddot{z} + 2\,\omega\,\dot{x} - 3\,\omega^2\, z = \frac{1}{m_c} F_z, \tag{1c}$$

with m_c being the mass of the chaser spacecraft and the angular frequency of the leader spacecraft $\omega = \sqrt{\mu/a^3}$ with μ being the Earth's standard gravitational parameter and a the semi-major axis of the leader satellite ([23], p. 40). Since Hill's equations are a set of time-invariant linear differential equations, they can be expressed in state-space form ($\dot{\vec{x}} = A\,\vec{x} + B\,\vec{u}$):

$$\dot{\vec{x}} = \begin{bmatrix} \dot{x}(t) \\ \dot{y}(t) \\ \dot{z}(t) \\ \ddot{x}(t) \\ \ddot{y}(t) \\ \ddot{z}(t) \end{bmatrix} = \begin{bmatrix} 0 & 0 & 0 & 1 & 0 & 0 \\ 0 & 0 & 0 & 0 & 1 & 0 \\ 0 & 0 & 0 & 0 & 0 & 1 \\ 0 & 0 & 0 & 0 & 0 & 2\omega \\ 0 & -\omega^2 & 0 & 0 & 0 & 0 \\ 0 & 0 & 3\omega^2 & -2\omega & 0 & 0 \end{bmatrix} \cdot \begin{bmatrix} x(t) \\ y(t) \\ z(t) \\ \dot{x}(t) \\ \dot{y}(t) \\ \dot{z}(t) \end{bmatrix}$$

$$+ \begin{bmatrix} 0 & 0 & 0 \\ 0 & 0 & 0 \\ 0 & 0 & 0 \\ 1 & 0 & 0 \\ 0 & 1 & 0 \\ 0 & 0 & 1 \end{bmatrix} \cdot \begin{bmatrix} u_x(t) \\ u_y(t) \\ u_z(t) \end{bmatrix}, \tag{2}$$

with the state vector $\vec{x}(t)$ and total external accelerations or control vector $\vec{u}(t) = [u_x,\, u_y,\, u_z]^T = \frac{\vec{F}}{m_c}$ ([23], p. 40f).

2.3. Graph Theory Fundamentals

Interconnection topologies between satellites or agents in a distributed control system can most adequately be described using graph theory. Thus the relevant terms and definitions later on used will be introduced.

2.3.1. Graph

A graph (or undirected graph) is an ordered pair $G = (V, E)$, where V is a set of vertices (or nodes) and E is a set of edges (see Figure 2). Each edge itself is an unordered pair of vertices. $e_{ij} = \{v_i, v_j\}$ e.g., describes the edge between the vertices v_i and v_j. For an undirected graph $e_{ij} = e_{ji}$ [24].

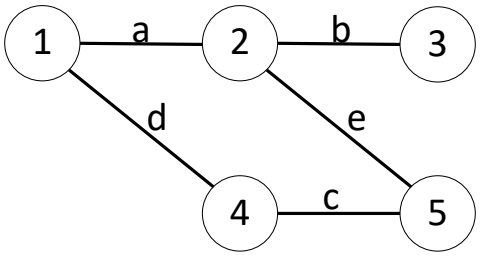

Figure 2. Undirected graph with its vertices are labeled with numbers and its edges with letters.

2.3.2. Directed Graph

A directed graph (or digraph) is a graph in which the edges have orientations (see Figure 3). Thus an edge is an ordered pair of two vertices. $e_{ij} = (v_i, v_j)$ then describes the edge from vertex v_i to vertex v_j. In general, for directed graphs $e_{ij} \neq e_{ji}$ [24].

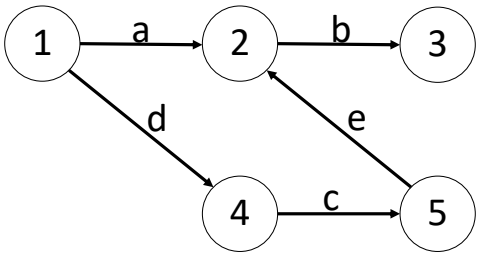

Figure 3. Directed graph with its vertices are labeled with numbers and its edges with letters. Edges show arrows to visualize their direction, e.g., *a* is the edge from vertex 1 to vertex 2.

2.3.3. Path

A path in a directed graph is an ordered sequence of vertices such that any consecutive pair within the sequence is an edge of the directed graph. In other words, a path is a walk through a graph from a vertex via vertices to a vertex along edges. The length of the path is defined by the number of consecutive edges in the path. Figure 4 visualizes a path within a graph [24].

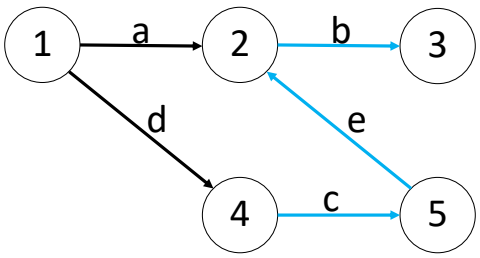

Figure 4. Directed graph with a path from vertex 4 to vertex 3 highlighted.

2.3.4. Reachability

A vertex v_i within a directed graph is said to be reachable from another vertex v_j, if there exists a path from v_j to v_j. A vertex is globally reachable, if there exists a path from every other vertex. A graph is said to be connected (strongly connected in case of directed graphs), if every vertex is globally reachable. Cf. Figure 4 as an example where vertex 3 is a globally reachable node, since it is reachable from every other vertex [24].

2.3.5. Neighbor

A vertex v_i is said to be a neighbor of vertex v_j, if there exists an edge $e_{ji} = (v_j,\ v_i)$ from vertex v_j to vertex v_i. For undirected graphs, if v_i is a neighbor of v_j then also v_j is a neighbor of v_i, e.g., in Figure 4 nodes 2 is a neighbor of node 1, but not the other way round [24].

2.3.6. Adjacency Matrix

Neighborhood relations within a graph can be expressed in an algebraic way as a matrix, the so called adjacency matrix $A_j = \left[a_{ij}\right] \in \mathbb{R}^{n\times n}$ with

$$a_{ij} = \begin{cases} 1 & \text{if } \exists\ e_{ij} = (v_i,\ v_j) \in E \\ 0 & \text{otherwise.} \end{cases} \tag{3}$$

A graph is undirected, if $a_{ij} = a_{ji}$ [24].

2.3.7. Degree Matrix

The degree matrix $D_g = \left[d_{ij}\right] \in \mathbb{R}^{n\times n}$ is a diagonal matrix stating the number of edges connected to each node. It is defined as

$$d_{ij} = \begin{cases} deg(v_i) & \text{if } i = j \\ 0 & \text{otherwise.} \end{cases} \tag{4}$$

where the degree $deg(v_i) = \sum_j a_{ij}$ counts the number of outgoing edges of a vertex v_i [24].

2.3.8. Laplacian Matrix

The Laplacian matrix $L \in \mathbb{R}^{n\times n}$ is a matrix representation of the graph. It combines adjacency and degree matrix and is defined as:

$$L = D_g - A_j. \tag{5}$$

To get a better understanding of its physical meaning we can consider the case that only relative measurement between the agents along the connected edges is available. In this case the relative measurement of agent i can be written using $L = \left[l_{ij}\right]$ as

$$y_i(t) = \sum_j l_{ij}\ x_j(t), \tag{6}$$

or in matrix form

$$y(t) = L\ x(t). \tag{7}$$

Thus it can be understood as a relative-measurement matrix [24].

2.4. Distributed Control

A distributed control system is a control system wherein individual controllers are distributed throughout a larger system. Thus it differs from non-distributed systems, that consist of a single controller at a central location. In a distributed control system, a set of controllers is connected via a communication network. According to Tian [24] common features of distributed control systems

are distributed interconnections, local control rules, scalability and of course cooperation among the agents. Since in a distributed control system there is no central controller, the cooperation among the agents is crucial for the functionality of the system. Another characteristic is the spatially distributed interconnection of the agents. Each agent/local controller thus does not only take information about its own state/output into account, but also considers the information of some other agents. Since they can be distributed among large distances also delays or package loss may play a role. Distributed control systems feature a local control rule. Because there is no centralized supervisor/controller, each agent makes its own decisions based on its own sensor inputs and the information provided by its neighboring agents. An advantage of a local control rule is the high fault-tolerance capability, since failing of a single or few agents will not stop the complete system from working. Another reason why a local control rule is beneficial is scalability. Since a local control rule uses only local information from the agent itself or from neighboring agents, it usually does not depend on the size of the whole system and thus allows for an arbitrary number of agents in the system. Scalability enables the adaption of the control system towards new applications without changing the underlying system. Further distributed control systems can be differentiated into homogeneous and heterogeneous systems depending on the types and characteristics of the agents, if they are equal or differ [24].

2.4.1. Connection to Graph Theory

In a distributed control system, the network topology or interconnection scheme can be modeled using directed graphs. Each vertex represents a subsystem or agent. If there is information flow (i.e., a communication link) from one agent to another, then there exists an edge with the same direction in the graph. If all communication links are bidirectional, the topology can be described by an undirected graph.

2.4.2. General State-Space Representation of a Distributed LTI System

A distributed linear time-invariant (LTI) control system Σ consisting of N subsystems Σ_i can be described as:

$$\Sigma = (\Sigma_1, \Sigma_2, ..., \Sigma_N)^T, \tag{8}$$

and a subsystem Σ_i is defined as:

$$\dot{x}_i = A_{ii}\, x_i + \sum_{i \neq j}^{N} A_{ij}\, x_j + B_{ii}\, u_i + \sum_{i \neq j}^{N} B_{ij}\, u_j \tag{9}$$

$$y_i = C_{ii}\, x_i + \sum_{i \neq j}^{N} C_{ij}\, x_j + D_{ii}\, u_i + \sum_{i \neq j}^{N} D_{ij}\, u_j, \tag{10}$$

with the time dependencies of $\dot{x}_i(t)$, $y_i(t)$, $x_i(t)$, $x_j(t)$, $u_i(t)$, $u_j(t)$ being omitted to improve readability. (For fundamentals about single LTI control systems the reader is referred to ([25], p. 72)). The terms A_{ii}, B_{ii}, C_{ii}, D_{ii} describe the behavior of the subsystem Σ_i itself, whereas the mixed terms A_{ij}, B_{ij}, C_{ij}, D_{ij} describe the influence of other subsystems Σ_j on the subsystem Σ_i. Thus the coupling terms can be named as

$$\sum_{i \neq j}^{N} A_{ij}\, x_j: \quad \text{state coupling} \qquad \sum_{i \neq j}^{N} B_{ij}\, u_j: \quad \text{input coupling}$$

$$\sum_{i \neq j}^{N} C_{ij}\, x_j: \quad \text{output coupling} \qquad \sum_{i \neq j}^{N} D_{ij}\, u_j: \quad \text{feed-through coupling.}$$

2.4.3. Decentralized and Distributed Control

A controller can be used to compute the control input for the distributed system Σ described in Equations (9) and (10), e.g., $u_i(t) = -K\ x_i(t)$. If the controller takes only the local state into account, meaning

$$u_i(t) = f(x_i(t)), \tag{11}$$

it is using a decentralized control approach. If it also takes states of other subsystems into account, meaning

$$u_i(t) = f(x_i(t), x_j(t), ...), \tag{12}$$

it is using a distributed control approach.

2.4.4. Distributed Consensus Approach

There are different types of distributed control systems. A promising way of cooperation in a distributed control system is finding a common agreement or consensus among the agents [24]. The distributed consensus approach is a method to compute the control input $u_i(t)$ of distributed systems Σ in which only the controllers, but not the plants are coupled. Figure 5 shows an exemplary block diagram for two coupled controllers with these characteristics. With respect to the general representation in Equations (9) and (10) the matrices A_{ij}, B_{ij}, C_{ij} and D_{ij} are equal $0\ \forall\ i \neq j$.

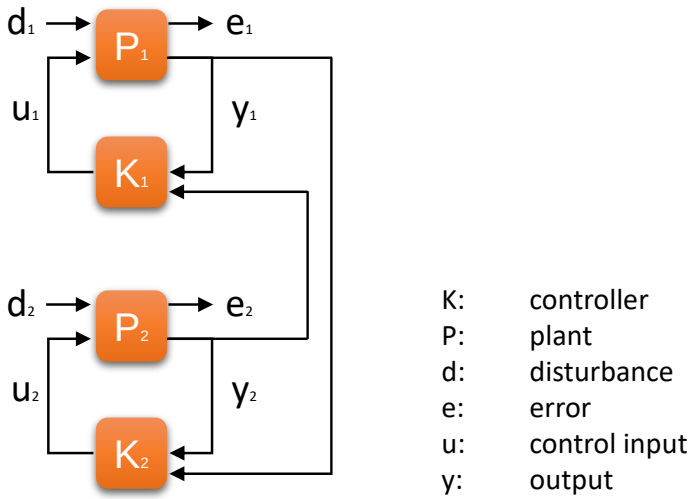

Figure 5. Two plants P_1 and P_2 with their controllers K_1 and K_2. The plants are not coupled, but the controllers are. Here, y_1 influences K_2 and y_2 influences K_1.

In this case, the control input can then be defined by a consensus protocol (for a regulator problem) by ([26], p. 26):

$$u_i(t) = K \sum_j a_{ij}\ (y_j(t) - y_i(t)), \tag{13}$$

where a_{ij} are the elements of the adjacency matrix A_j and K is a gain matrix for a single subsystem/agent. With the state-space definition of a single system $(A,\ B,\ C,\ 0)$ and by linking together the states of the subsystems $x = (x_1, x_2, ..., x_N)^T$ to form the state of the overall system the closed-loop system with consensus protocol can be written in matrix form as ([24], eq. 6.59):

$$\dot{x}(t) = (I_N \otimes A - L \otimes BKC)\ x(t), \tag{14}$$

where $\otimes$ denotes the Kronecker product, an operator on two matrices defined as

$$A \otimes B = \begin{pmatrix} a_{11}\, B & \dots & a_{1m}\, B \\ \vdots & & \vdots \\ a_{n1}\, B & \dots & a_{nm}\, B, \end{pmatrix} \tag{15}$$

with the properties

$$(A \otimes B) \cdot (C \otimes D) = (A \cdot C) \otimes (B \cdot D) \tag{16}$$

$$A \otimes (B + C) = A \otimes B + A \otimes C \tag{17}$$

$$A \otimes B \neq B \otimes A \quad \text{(in general)} \tag{18}$$

$$A \otimes (B \otimes C) = (A \otimes B) \otimes C \tag{19}$$

$$(\alpha_A A \otimes \alpha_B B) = \alpha_A\, \alpha_B\, (A \otimes B). \tag{20}$$

This control approach enforces the satellites to reduce the relative distances/vectors along all interconnections.

2.4.5. Reference Tracking

The consensus protocol for regulation problems presented in Equation (13) can be adapted for reference tracking problems:

$$u_i(t) = K \sum_j a_{ij} \left[r_{ji} - (y_j(t) - y_i(t)) \right], \tag{21}$$

with r_{ji} being the reference vector from satellite i to satellite j. Obviously, $r_{ij} = -r_{ji}$ and $r_{ii} = 0$. Figure 6 shows an exemplary block diagram of three systems with controllers coupled via the consensus approach.

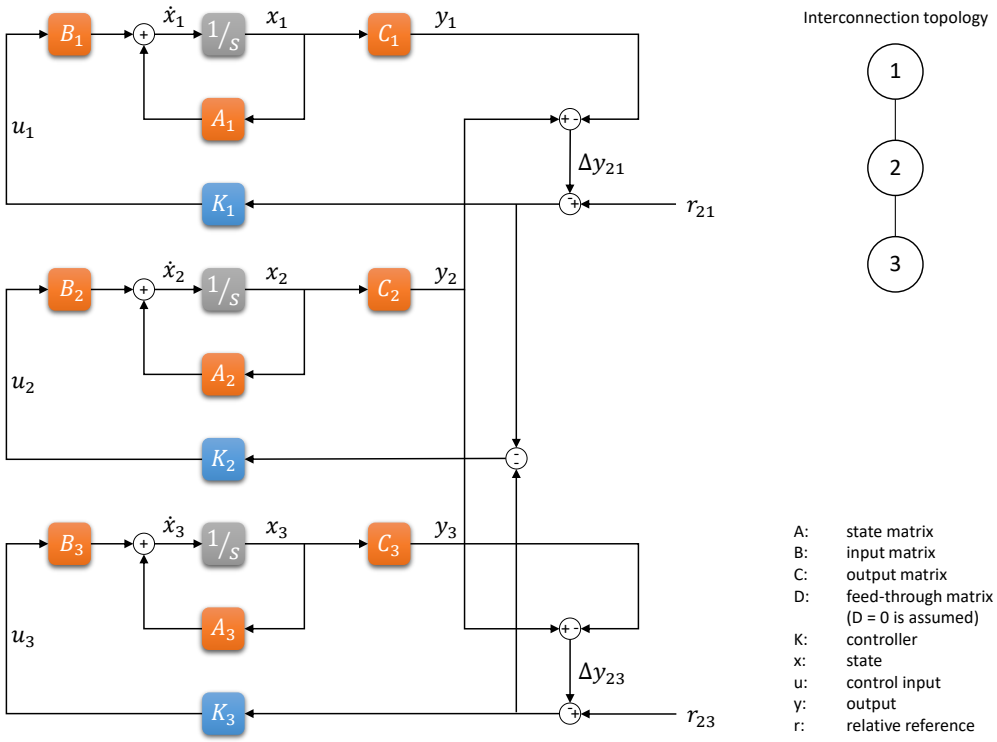

Figure 6. Exemplary block diagram of three distributed systems with their controllers coupled via the consensus approach. The interconnection topology is shown as a graph in the upper right corner.

Additionally, Figure 7 presents a schematic explaining the relative references r_{ij} provided to the distributed controllers as stated in Equation (21).

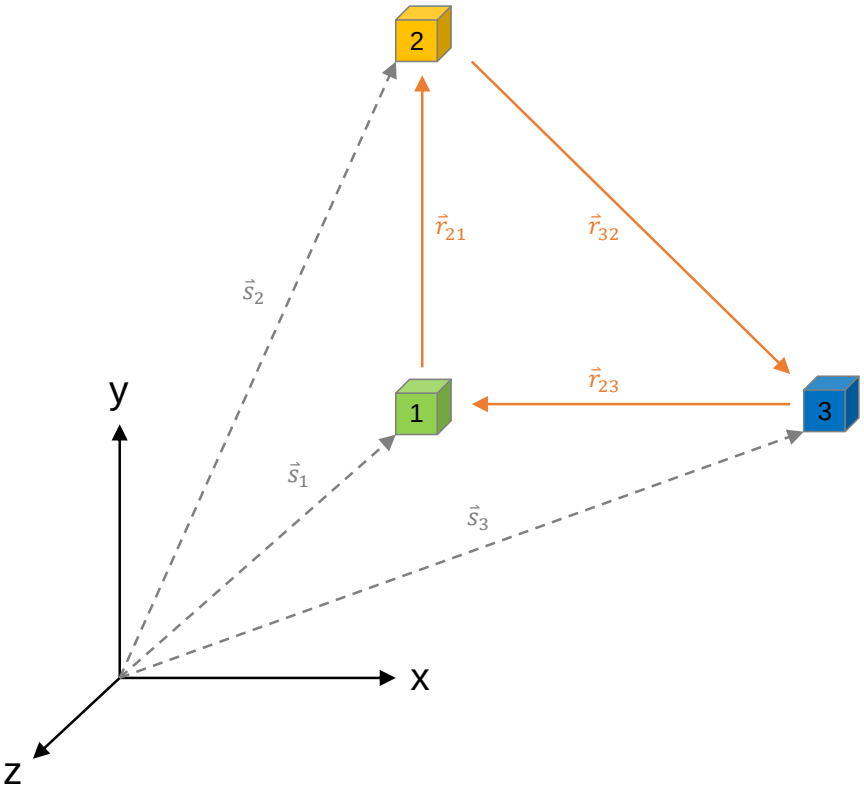

Figure 7. Schematic drawing of three agents in an arbitrary coordinate system. Their states are labeled $\vec{s}_1$, $\vec{s}_2$ and $\vec{s}_3$. Relative references are labeled according to Equation (21) with $\vec{r}_{ji}$ being the reference vector from agent i to agent j. For readability, the inverse references $\vec{r}_{ij} = -\vec{r}_{ji}$ are omitted.

To reformulate Equation (21) in matrix form the references r_{ij} can be organized in a matrix:

$$R = \begin{pmatrix} 0 & r_{12} & r_{13} & r_{14} \\ -r_{12} & 0 & r_{23} & r_{24} \\ -r_{13} & -r_{23} & 0 & r_{34} \\ -r_{14} & -r_{24} & -r_{34} & 0 \end{pmatrix}. \tag{22}$$

R is skew-symmetric and has the same zero-values as the adjacency matrix A_j. Using R, the closed-loop system of this extended tracking problem can also be written in matrix form:

$$\dot{x}(t) = \\ (I_N \otimes A)\, x(t) - \left\{ (L \otimes BKC) \odot \left[\left(1_{6\times 1} \otimes x^T(t) \right) + (R \otimes 1_{6\times 1}) \right] \right\} \cdot 1_{N\cdot 6\times 1} \tag{23}$$

or

$$\dot{x}(t) = \\ (I_N \otimes A - L \otimes BKC)\, x(t) + \left[(L \otimes BKC) \odot (R \otimes 1_{6\times 1}) \right] \cdot 1_{N\cdot 6\times 1}, \tag{24}$$

where $\odot$ denotes the Hadamard product (or element-wise product) of two matrices, which is defined for two matrices A and B with equal size $(n \times m)$ by

$$A \odot B = (a_{ij} \cdot b_{ij}) = \begin{pmatrix} a_{11} \cdot b_{11} & \cdots & a_{1m} \cdot b_{1m} \\ \vdots & \ddots & \vdots \\ a_{n1} \cdot b_{n1} & \cdots & a_{nm} \cdot b_{nm} \end{pmatrix}. \tag{25}$$

The aim of formation control is that all agents follow a predefined or given trajectory while maintaining a particular spacial formation. Thus, the consensus approach is especially suitable for formation control.

2.4.6. Fixing Coordinate Origin to an Agent

In some cases, e.g., for easier measuring of the states of the involved agents and easier definition of the coordinate frame origin, it makes sense to fix the coordinate frame origin to one agent's position. This means that the state of this agent, called leader, is always zero. The leader then is passive and no control input should be applied to him to control the internal structure of the formation. To enable this, the interconnection graph has to be directed and the adjacency matrix has to be asymmetric. Connections to the leader are possible, but connections from the leader are forbidden. This leads to the following condition for the elements of an adjacency matrix A_j and a fixed, passive leader l.

$$a_{ij} = 0 \iff i = l. \tag{26}$$

2.5. Robust Control

Robust control is a branch of control theory that explicitly deals with uncertainty. A controller designed for a particular set of parameters is said to be robust, if it would also work well under a different set of assumptions. Rather than adapting to variations of measurements, the controller is designed to work assuming that certain variables will be unknown, but bounded. H_∞ loop-shaping is an typical example. Figure 8 presents a block diagram of a general control configuration in a robust setup.

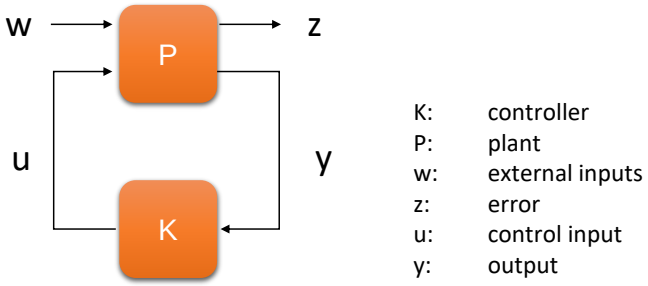

Figure 8. General control configuration ([27], p. 442).

A generalized plant including external inputs w, errors z, control inputs u and outputs y can be represented as a general state-space model with the state x and its derivation $\dot{x}$ as internal variables:

$$\begin{aligned} \dot{x} &= A\,x + B_1\,w + B_2\,u \\ z &= C_1\,x + D_{11}\,w + D_{12}\,u \\ y &= C_2\,x + D_{21}\,w + D_{22}\,u. \end{aligned} \tag{27}$$

External inputs w can contain various inputs from a reference signal r to disturbances d to noise n. The state-space model can be—as every control system expressed in a state-space representation—transformed into a transfer function (TF) ([27], p. 442), ([28], p. 20). (The inverse transformation from a TF $P(s)$ to a state-space model (A, B, C, D) cannot be formulated in a general formula, but is dependent on the order of the system and the number of inputs and outputs. Different procedures can be applied to compute this transformation. Depending on the procedure, either the observability canonical form, controllability canonical form or the diagonalized form of a state-space model can be obtained ([29], p. 119).) The transformation from a state-space model to a TF can be performed using

$$P(s) = C(sI - A)^{-1}B + D \tag{28}$$

as

$$P(s) = \begin{array}{c} \\ z \\ y \end{array} \overset{\begin{array}{cc} w & u \end{array}}{\left(\begin{array}{c|c} P_{11}(s) & P_{12}(s) \\ \hline P_{21}(s) & P_{22}(s) \end{array}\right)}. \tag{29}$$

With the help of Equation (28), we introduce the notation

$$P(s) = \begin{array}{c} \\ \dot{x} \\ z \\ y \end{array} \overset{\begin{array}{ccc} x & w & u \end{array}}{\left(\begin{array}{c|cc} A & B_1 & B_2 \\ \hline C_1 & D_{11} & D_{12} \\ C_2 & D_{21} & D_{22} \end{array}\right)}, \tag{30}$$

which implies Equation (28) and translates the state-space representation to a TF ([27], p. 442).

2.5.1. H_∞ Control

The H_∞ control approach considers the H_∞ norm of the closed-loop transfer function (CLTF)

$$T_{zw} = F_L(P, K), \tag{31}$$

with F_L representing the lower linear fractional transformation (LFT) [30]. It is defined for a given complex matrix M and a given rational matrix Δ_L with

$$M = \begin{pmatrix} M_{11} & M_{12} \\ M_{21} & M_{22} \end{pmatrix} \tag{32}$$

as

$$F_L(M, \Delta_L) := M_{11} + M_{12}\Delta_L \left(I - M_{22}\Delta_L\right)^{-1} M_{21}. \tag{33}$$

The H_∞ control problem can be defined as finding a stabilizing controller that (1) minimizes

$$\|T_{zw}\|_\infty \tag{34}$$

(optimal control problem) or (2) with

$$\|T_{zw}\|_\infty < \gamma, \gamma > 0 \tag{35}$$

(suboptimal control problem) ([27], p. 443).

2.6. Distributed Robust Control

In this section, a combination of distributed control using the consensus approach and robust H_∞-control as defined in the previous sections is presented. The main objectives of control are reference

tracking for acquiring a given relative formation topology, together with disturbance rejection (e.g., errors of actuator systems) under the presence of (sensor) noise. In addition, the required control input should be optimized. Thus a mixed sensitivity approach is chosen, which is presented in the following section.

2.6.1. Mixed Sensitivity Closed-Loop System with Distributed Controller Interconnections

Based on the work presented in Section 2.4.4 and in Figure 6 on the distributed consensus approach and especially on and Equation (21), which describes the consensus protocol for reference tracking, we first compile a block diagram of the closed-loop system of a single agent i with mixed sensitivity robustness and an arbitrary number n of interconnections to other agents' controllers. This is presented in Figure 9.

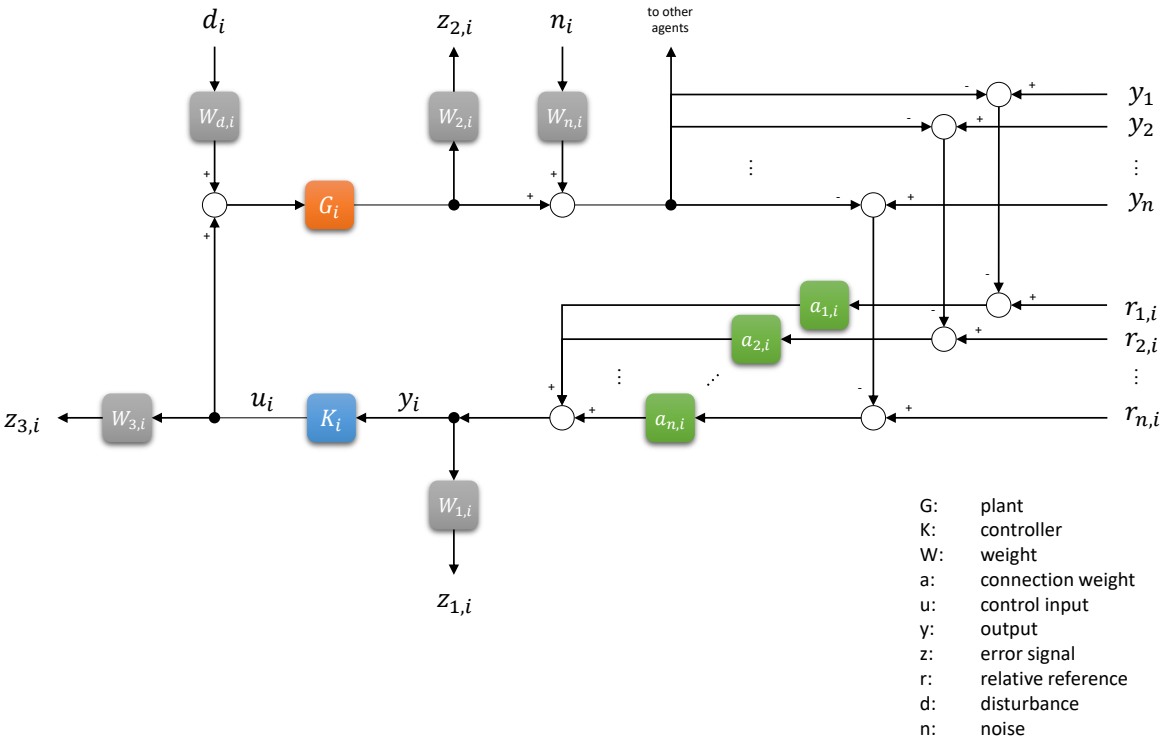

Figure 9. Mixed sensitivity closed-loop system with distributed controller interconnections.

2.6.2. Obtaining Generalized Plant for Single Agent

From the block diagram in Figure 9 the complete generalized plant for mixed sensitivity with distributed consensus based reference inputs for agent i with interconnections to n other agents can be derived:

$$P_i = \begin{array}{c|c} & \begin{array}{cccccc|c} d & n & y_1 & y_2 \dots y_n & r_{1i} & r_{2i} \dots r_{ni} & u \end{array} \\ \hline \begin{array}{c} z_1 \\ z_2 \\ z_3 \\ \hline y \end{array} & \left(\begin{array}{cccccc|c} W_1\, A_i\, G_i\, W_d & W_1\, A_i\, W_n & -W_1\, a_{1i} & \dots & W_1\, a_{1i} & \dots & W_1\, A_i\, G_i \\ W_2\, G_i\, W_d & 0 & 0 & 0 & 0 & 0 & W_2\, G_i \\ 0 & 0 & 0 & 0 & 0 & 0 & W_3 \\ \hline A_i\, G_i\, W_d & A_i\, W_n & -a_{1i} & \dots & a_{1i} & \dots & A_i\, G_i \end{array} \right) \end{array}, \quad (36)$$

with y being the output of agent i, d the disturbance and n the noise. a_{ji} is the weight on the connection from agent j to agent i. In general case $a_{ji} \neq a_{ij}$, though in practical applications communication

between agents often is bidirectional, which leads to $a_{ji} = a_{ij}$. Further, $A_i = \sum_j a_{ji}$ and r_{ji} is the reference for the relative state from agent j to agent i. Further $G_d = G_i$ is assumed here.

2.6.3. Computation of the CLTF

The CLTF T_{zw} of an agent i can be computed by combining the generalized plant description given in Equation (36) with a controller K_i using a lower LFT. By dividing the overall matrix into four block matrices M_{ij} Equation (36) can be reformulated to

$$P_i = \begin{array}{c} \\ z \\ y \end{array} \overset{\begin{array}{cc} d/n/y/r & u \end{array}}{\left(\begin{array}{c|c} M_{11} & M_{12} \\ \hline M_{21} & M_{22} \end{array}\right)}. \tag{37}$$

The CLTF T_{zw} can be computed by combining the above matrix and the controller K_i in a lower LFT:

$$T_{zw} = F_L(P_i, K_i) = M_{11} + M_{12} K_i \left(I - M_{22} K_i\right)^{-1} M_{21}. \tag{38}$$

By introducing the sensitivity $S_i^* = (I - M_{22} K_i)^{-1} = (I - A_i G_i K_i)^{-1}$ the CLTF can be expressed as

$$T_{zw} = \begin{array}{c} \\ z_1 \\ z_2 \\ z_3 \end{array} \overset{\begin{array}{cccccc} d & n & y_1 & y_2 \dots y_n & r_{1i} & r_{2i} \dots r_{ni} \end{array}}{\begin{pmatrix} W_1 A_i G_i W_d + W_1 A_i G_i K_i S_i A_i G_i W_d & W_1 A_i W_n + W_1 A_i G_i K_i S_i A_i W_n & -W_1 a_{1i} - W_1 A_i G_i K_i S_i a_{1i} & & W_1 a_{1i} + W_1 A_i G_i K_i S_i a_{1i} & \\ W_2 G_i W_d + W_2 G_i K_i S_i A_i G_i W_d & W_2 G_i K_i S_i A_i W_n & -W_2 G_i K_i S_i a_{1i} & \dots & W_2 G_i K_i S_i a_{1i} & \dots \\ W_3 K_i S_i A_i G_i W_d & W_3 K_i S_i A_i W_n & -W_3 K_i S_i a_{1i} & & W_3 K_i S_i a_{1i} & \end{pmatrix}}. \tag{39}$$

This equation can be simplified using the identities $1 + A_i G_i K_i S_i = S_i$ and $G_i K_i S_i = T_i$ (derived from the definition of the sensitivity function $S = (I + G K)^{-1}$ and the complementary sensitivity function $T = (I + G K)^{-1} G K$, cf. ([29], p. 22)):

$$T_{zw} = \begin{array}{c} \\ z_1 \\ z_2 \\ z_3 \end{array} \overset{\begin{array}{cccccc} d & n & y_1 & y_2 \dots y_n & r_{1i} & r_{2i} \dots r_{ni} \end{array}}{\begin{pmatrix} W_1 S_i A_i G_i W_d & W_1 S_i A_i W_n & -W_1 S_i a_{1i} a_{1i} & & W_1 S_i a_{1i} & \\ W_2 (1 + G_i K_i S_i A_i) G_i W_d & W_2 T_i A_i W_n & -W_2 T_i a_{1i} & \dots & W_2 T_i a_{1i} & \dots \\ W_3 K_i S_i A_i G_i W_d & W_3 K_i S_i A_i W_n & -W_3 K_i S_i a_{1i} & & W_3 K_i S_i a_{1i} & \end{pmatrix}}. \tag{40}$$

By further assuming $A_i = \alpha \cdot I$ (which is equivalent to the fact that a_{ji} weights connections between agents and not channels individually), we can use the identity $A_i \cdot X = X \cdot A_i$ and simplify the element $(2,1)$ of T_{zw}, which is the TF $T_{z_2,d}$. Further it is to note that, if $A_i = -I$, which means that there is no gain on the connections between the agents, the CLTF simplifies to

$$T_{zw} = \begin{array}{c} \\ z_1 \\ z_2 \\ z_3 \end{array} \overset{\begin{array}{cccccc} d & n & y_1 & y_2 \dots y_n & r_{1i} & r_{2i} \dots r_{ni} \end{array}}{\begin{pmatrix} -W_1 S_i G_i W_d & -W_1 S_i W_n & -W_1 S_i a_{1i} a_{1i} & & W_1 S_i a_{1i} & \\ W_2 S_i G_i W_d & -W_2 T_i W_n & -W_2 T_i a_{1i} & \dots & W_2 T_i a_{1i} & \dots \\ -W_3 K_i S_i G_i W_d & -W_3 K_i S_i W_n & -W_3 K_i S_i a_{1i} & & W_3 K_i S_i a_{1i} & \end{pmatrix}}, \tag{41}$$

which is identical to the classical mixed sensitivity CLTF of a single system (except of the additional reference inputs y_i and $r_{ji}, j \neq i$ and renaming a_{1i} to W_r).

2.6.4. Obtaining the Generalized Plant for the Overall System

Starting from the plant description of the distributed systems or agents in Equation (36), we now compose the general plant of the overall system P. Thus we define $A = diag(A_1, A_2, ..., A_n)$ with $A_i = \sum_j a_{ji}$. We further assume that the individual agents are equal. Thus

$$\begin{array}{lll} G = G_i & W_1 = W_{1,i} & W_2 = W_{2,i} \\ W_3 = W_{3,i} & W_d = W_{d,i} & W_n = W_{n,i} \ \forall\, i. \end{array} \tag{42}$$

The general plant description can then be composed of the P_i of the individual agents under the given assumptions to:

$$P = \begin{array}{c|cccccccccc|cc} & d_1 & d_2 & \dots & n_1 & n_2 & \dots & r_{11} & r_{21} & r_{31} & \dots & r_{12} & \dots & u_1 & u_2 & \dots \\ z_{1|1} & W_1\,A_1\,G\,W_d & -W_1\,a_{21}\,G\,W_d & & W_1\,A_1\,W_n & 0 & & 0 & W_1\,a_{21} & W_1\,a_{31} & & 0 & & W_1\,A_1\,G & -W_1\,a_{21}\,G & \\ z_{1|2} & -W_1\,a_{12}\,G\,W_d & W_1\,A_2\,G\,W_d & & 0 & W_1\,A_2\,W_n & & 0 & 0 & 0 & & W_1\,a_{12} & & -W_1\,a_{12}\,G & W_1\,A_2\,G & \\ \vdots & & & & & & & & & & & & & & & \\ z_{1|n} & -W_1\,a_{1n}\,G\,W_d & -W_1\,a_{n1}\,G\,W_d & & 0 & 0 & & 0 & 0 & 0 & & 0 & & -W_1\,a_{1n}\,G & -W_1\,a_{2n}\,G & \\ z_{2|1} & W_2\,G\,W_d & 0 & & 0 & 0 & & 0 & 0 & 0 & & 0 & & W_2\,G & 0 & \\ z_{2|2} & 0 & W_2\,G\,W_d & & 0 & 0 & & 0 & 0 & 0 & & 0 & & 0 & W_2\,G & \\ \vdots & & & & & & & & & & & & & & & \\ z_{2|n} & 0 & 0 & & 0 & 0 & & 0 & 0 & 0 & & 0 & & 0 & 0 & \\ z_{3|1} & 0 & 0 & & 0 & 0 & & 0 & 0 & 0 & & 0 & & W_3 & 0 & \\ z_{3|2} & 0 & 0 & & 0 & 0 & & 0 & 0 & 0 & & 0 & & 0 & W_3 & \\ \vdots & & & & & & & & & & & & & & & \\ z_{3|n} & 0 & 0 & & 0 & 0 & & 0 & 0 & 0 & & 0 & & 0 & 0 & \\ y_1 & A_1\,G\,W_d & -a_{21}\,G\,W_d & & A_1\,W_n & 0 & & 0 & a_{21} & a_{31} & & 0 & & A_1\,G & -a_{21}\,G & \\ y_2 & -a_{12}\,G\,W_d & A_2\,G\,W_d & & 0 & A_2\,W_n & & 0 & 0 & 0 & & a_{12} & & -a_{12}\,G & A_2\,G & \\ \vdots & & & & & & & & & & & & & & & \\ y_n & -a_{1n}\,G\,W_d & -a_{n1}\,G\,W_d & & 0 & 0 & & 0 & 0 & 0 & & 0 & & -a_{1n}\,G & -a_{2n}\,G & \end{array} \tag{43}$$

To reduce the size and increase the readability and usability of this matrix, we can combine different parts of it as matrices. Thus we use the Kronecker product $\otimes$ with its properties defined in Equations (15)–(20) and the Hadamard product $\odot$ as defined in Equation (25). Further, let $A_i = \sum_j a_{ji}$ (this can be understood as the effect of all weights $a_j i, j = 1...n$ on the output y_i of a system i before entering the controller K_i) and

$$A_d = \begin{pmatrix} A_1 & \dots & 0 \\ \vdots & \ddots & \vdots \\ 0 & \dots & A_n \end{pmatrix} \tag{44}$$

$$A_a = \begin{pmatrix} 0 & a_{2,1} & \dots & a_{n-1,1} & a_{n,1} \\ a_{1,2} & 0 & & & a_{n,2} \\ \vdots & & \ddots & & \vdots \\ a_{1,n-1} & & & 0 & a_{n,n-1} \\ a_{1,n} & a_{2,n} & \dots & a_{n-1,n} & 0 \end{pmatrix}. \tag{45}$$

and

$$L = A_d - A_a. \tag{46}$$

For better readability we define the unit matrices

$$I_n = \begin{pmatrix} 1 & & & & \\ & 1 & & & \\ & & \ddots & & \\ & & & 1 & \\ & & & & 1 \end{pmatrix}_{n \times n} \tag{47}$$

and

$$I_{a \times b} = \begin{pmatrix} 1 & \dots & 1 \\ \vdots & \ddots & \vdots \\ 1 & \dots & 1 \end{pmatrix}. \tag{48}$$

Now we can rewrite Equation (43) with inputs and outputs in vector form as

$$P = \begin{array}{c|ccc|c} & \vec{d} & \vec{n} & \vec{r} & \vec{u} \\ \vec{z_1} & (1_n \otimes W_1) \cdot L \cdot (1_n \otimes (G\, W_d)) & (1_n \otimes W_n) \cdot A_d \cdot (1_n \otimes W_n) & (1_{1\times n} \otimes ((1_n \otimes W_1) \cdot A_d)) \odot (1_n \otimes 1_{s\times sn}) & (1_n \otimes W_1) \cdot L \cdot (1_n \otimes G) \\ \vec{z_2} & 1_n \otimes (W_2\, G\, W_d) & 0 & 0 & 1_n \otimes (W_2\, G) \\ \vec{z_3} & 0 & 0 & 0 & 1_n \otimes W_3 \\ \hline \vec{y} & L \cdot (1_n \otimes (G\, W_d)) & A_d \cdot (1_n \otimes W_n) & (1_{1\times n} \otimes A_d) \odot (1_n \otimes 1_{s\times sn}) & L \cdot (1_n \otimes G) \end{array}, \quad (49)$$

with n being the number of agents or subsystems and s the number of states per subsystem (or alternatively $s \cdot n$ the total number of states of the overall system). Now we have a general plant description of a distributed multi-agent system using consensus control that can be applied to H_∞ synthesis.

It has to be noted that the matrix giving the general plant description of the overall system in Equation (49) grows with the number of agents. Thus using this equation is not suitable for large scale systems with hundreds or thousands of agents, since it will not be possible to find numerical solutions for extremely large matrices. However, Equation (36) which describes the generalized plant of a single agent only scales with the number of interconnected agents and thus can be used also in large scale systems as long as the number of interconnected neighbors remains small.

3. Results

This chapter contains simulation results on a realistic space scenario performed with MathWorks MATLAB (Version 2018b) together with the Robust Control Toolbox. Scenario definition, formation topology, controller synthesis and simulation results are presented.

3.1. Scenario Definition

We will consider the following example: five satellites form a spaceborne distributed telescope. Four satellites are situated in an equilateral square in the x–y plane of the LVLH coordinate frame representing the mirrors of a telescope. One satellite is located above the center of the square shifted towards –z direction representing the sensor of the telescope. This scenario is loosely based on ESA's Darwin study that aimed at detecting Earth-like planets orbiting nearby stars by collecting infrared light with several satellites placed at the Lagrange point L2 and combining it in one satellite using interferometry (cf. Figure 10). In contrast to Darwin, we place the satellites in a low Earth orbit (LEO) and make use of Hill's equations. The position, where such a spaceborne telescope would be placed, depends mainly on the scientific aim of the observation (which is out of scope of this work). However, a LEO is of higher interest for other SFF missions and thus preferred as example. The formation will be under the influence of orbit dynamics (cf. Equation (1)) which will lead to a decay of the formation topology. Thus, continuous control is required for maintaining it. Further, we do not assume global knowledge in the sense that each spacecraft has a communication link and state exchange with every other spacecraft, but only with its neighbors.

To present a realistic robust control example, we further assume disturbances acting on the satellite. We assume a Gaussian distributed force acting on the satellite with a magnitude of 50 µN (standard normal distribution). This force represents thruster uncertainties of a typical electric propulsion system.

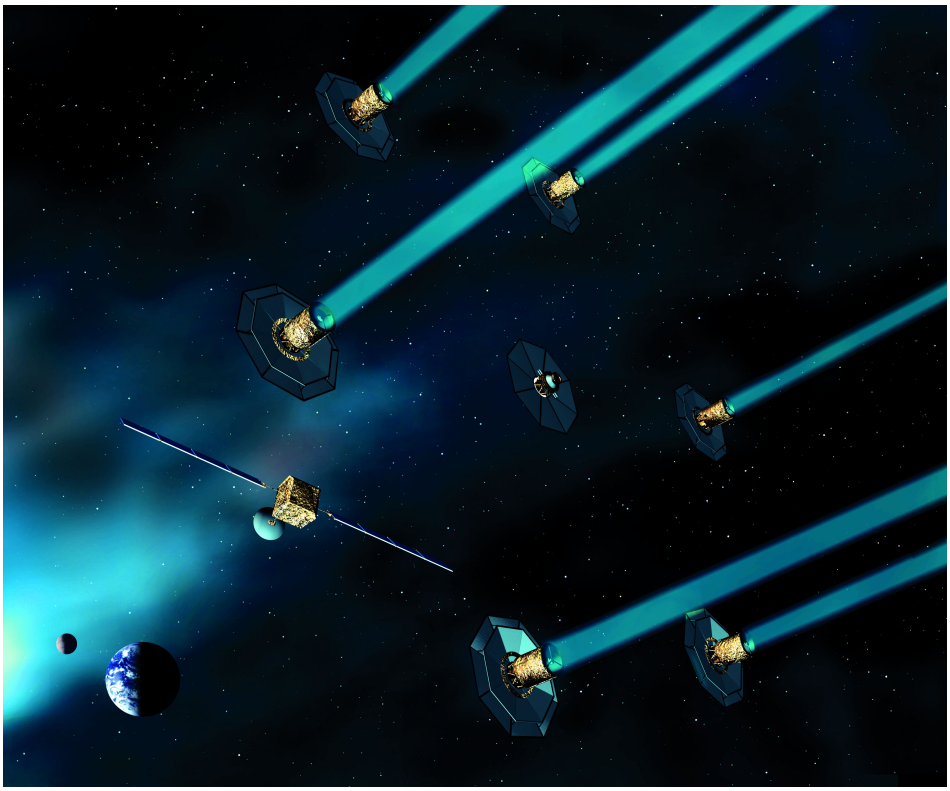

Figure 10. Artificial drawing of ESA's Darwin mission study. (Image: ESA/Darwin, 2002, http://www.esa.int/spaceinimages/Images/2002/11/Darwin_will_combine_light_from_four_or_five_telescopes_and_send_it_down_to_Earth).

3.1.1. Network Topology

The network topology of this example is visualized in Figure 11. Since every vertex of the interconnection graph/agent except of number (5) is only connected to all but one other vertex/agent, the graph is not fully interconnected or complete. Based on the graph, the degree matrix D, which states the number of interconnections of the subsystems/agents, and the adjacency matrix A_j, which non-zero elements represent the interconnections, can be composed:

$$D = \begin{pmatrix} 3 & 0 & 0 & 0 & 0 \\ 0 & 3 & 0 & 0 & 0 \\ 0 & 0 & 3 & 0 & 0 \\ 0 & 0 & 0 & 3 & 0 \\ 0 & 0 & 0 & 0 & 4 \end{pmatrix} \tag{50}$$

$$A_j = \begin{pmatrix} 0 & 1 & 0 & 1 & 1 \\ 1 & 0 & 1 & 0 & 1 \\ 0 & 1 & 0 & 1 & 1 \\ 1 & 0 & 1 & 0 & 1 \\ 1 & 1 & 1 & 1 & 0 \end{pmatrix} \tag{51}$$

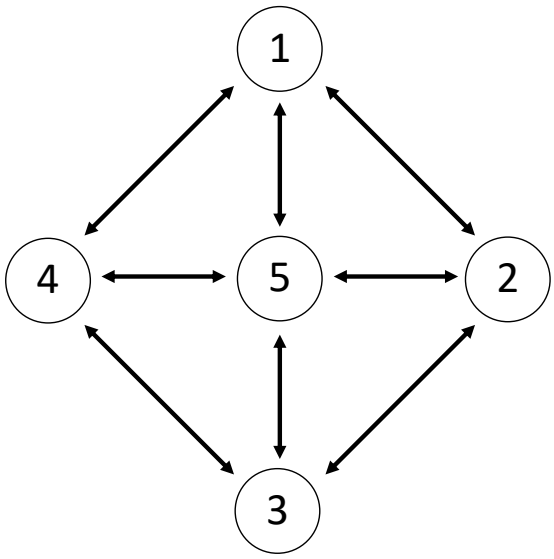

Figure 11. Interconnection graph of five satellites in a spaceborne telescope example. Interconnections between satellites are assumed to be bidirectional.

From D and A_j the Laplacian matrix can be computed to

$$L = D - A_j = \begin{pmatrix} 3 & -1 & 0 & -1 & -1 \\ -1 & 3 & -1 & 0 & -1 \\ 0 & -1 & 3 & -1 & -1 \\ -1 & 0 & -1 & 3 & -1 \\ -1 & -1 & -1 & -1 & 4 \end{pmatrix}. \tag{52}$$

3.1.2. Dynamically Decoupled State Definition

We can define the states of the spacecraft as their position and velocity in LVLH coordinate frame in a dynamically decoupled way (the definition of decoupled states feels natural, though it is not unique. One could also define the state in a coupled manner e.g., by taking the relative vectors between the satellites instead of the absolute position and velocity in the LVLH frame. The state of satellite 1 would then consist of the relative position and velocity vectors to all other connected satellites. However, this state definition would not be minimal any more).

$$\boldsymbol{x}_i = (x_i,\ \dot{x}_i,\ y_i,\ \dot{y}_i,\ z_i,\ \dot{z}_i)^T. \tag{53}$$

So the state of each satellite contains only local information of the satellite itself. Since the states of the satellites are not coupled and the satellites are not physically interconnected (the assumption that the satellites are not physically interconnected and thus $A_{ij} = B_{ij} = C_{ij} = D_{ij} = 0\ \forall\ i \neq j$ is only valid as long as some weaker physical effects are neglected. Examples are microgravity, the momentum transfer on a satellite caused by the propellant of other satellites or electric or magnetic repulsion or attraction. Such effects would lead to $A_{ij} \neq 0$ or $B_{ij} \neq 0$ and are partly nonlinear), there is no influence of the state or the control inputs of other satellites on the satellite itself. Thus $A_{ij} = B_{ij} = C_{ij} = D_{ij} = 0\ \forall\ i \neq j$ and we can reduce the general state-space model in Equations (9) and (10) to

$$\begin{aligned} \dot{x}_i(t) &= A_i\ x_i(t) + B_i\ u_i(t) \\ y_i(t) &= C_i\ x_i(t) + D_i\ u_i(t). \end{aligned} \tag{54}$$

Further, we can assume in this example that the matrices A_i and B_i are identical for all satellites, since they all share the same dynamic model and that $D = 0$ (assuming there is no feed-through of control input). This leads to:

$$\begin{aligned} \dot{x}_i(t) &= A\, x_i(t) + B\, u_i(t) \\ y_i(t) &= C_i\, x_i(t) \end{aligned} \tag{55}$$

The distributed control problem now consists of finding appropriate control inputs $u_i(t) = f(\dot{x}_i(t), \dot{x}_j(t))$.

3.1.3. Distributed Robust Consensus Approach

As we can see from the previous section (Equation (55)) the control problem can be formulated as a distributed state-space system. Thus, a distributed robust consensus approach as derived in Section 2.6.3 can be applied. Equation (41) presents the CLTF of an individual agent in a distributed control scenario and is applied in the presented scenario (Note that this approach does not control the position of the center of the formation. It only controls the relative vectors within the formation. Due to disturbances, the center of the formation might move with time, but the shape of the formation will be kept constant. Further, since relative vectors are defined with respect to a basis of a vector space, namely the axes of the LVLH coordinate frame, the orientation of the formation is fixed with respect to these axes). The system was modeled in Matlab including the aforementioned disturbance inputs d on all satellites, which represent thruster uncertainties of a typical electric propulsion system for small satellites with a maximum thrust force in the order of few 100 µN. We define the input weight for disturbance as a static scaling gain

$$W_d = 50 \cdot 10^{-6} \cdot I_3 \tag{56}$$

and the input weight for reference also as a static gain

$$W_r = I_6 \tag{57}$$

The output weights are defined as first-order weighting function with specified DC gain, crossover frequency, and high-frequency gain. Their TFs are defined as

$$W_1 = \begin{pmatrix} 1 & 0 & 0 & 0 & 0 & 0 \\ 0 & 0 & 0 & 0 & 0 & 0 \\ 0 & 0 & 1 & 0 & 0 & 0 \\ 0 & 0 & 0 & 0 & 0 & 0 \\ 0 & 0 & 0 & 0 & 1 & 0 \\ 0 & 0 & 0 & 0 & 0 & 0 \end{pmatrix} \cdot \frac{60.2\, s + 0.802}{s + 0.0802} \tag{58}$$

$$W_2 = \begin{pmatrix} 1 & 0 & 0 & 0 & 0 & 0 \\ 0 & 0 & 0 & 0 & 0 & 0 \\ 0 & 0 & 1 & 0 & 0 & 0 \\ 0 & 0 & 0 & 0 & 0 & 0 \\ 0 & 0 & 0 & 0 & 1 & 0 \\ 0 & 0 & 0 & 0 & 0 & 0 \end{pmatrix} \cdot \frac{10\, s + 13.27}{s + 16.58} \tag{59}$$

$$W_3 = \begin{pmatrix} 1 & 0 & 0 \\ 0 & 1 & 0 \\ 0 & 0 & 1 \end{pmatrix} \cdot \frac{s + 0.1}{s + 10}. \tag{60}$$

The robust control problem is now defined as finding a stabilizing controller that minimizes the H_∞ norm of the CLTF with external inputs (disturbance d, references r) and output error signals (z_1, z_2

and z_3) T_{zw} or (as the suboptimal control problem that can be solved numerically, cf. Section 2.5.1 and Equation (35)) as finding a stabilizing controller with

$$\|T_{zw}\|_\infty < \gamma, \gamma > 0.$$

In addition to that, we impose constraints on the structure of the sought controller in order to limit its complexity. As a reasonable compromise between performance and complexity, we require the controller to be a state-space system with six states, six inputs and tree outputs:

$$A_c = \begin{pmatrix} a_{11} & \cdots & a_{16} \\ \vdots & \ddots & \vdots \\ a_{61} & \cdots & a_{66} \end{pmatrix} \qquad B_c = \begin{pmatrix} b_{11} & \cdots & b_{16} \\ \vdots & \ddots & \vdots \\ b_{61} & \cdots & b_{66} \end{pmatrix}$$
$$C_c = \begin{pmatrix} a_{11} & \cdots & a_{16} \\ \vdots & \ddots & \vdots \\ a_{31} & \cdots & a_{36} \end{pmatrix} \qquad D_c = \begin{pmatrix} a_{11} & \cdots & a_{16} \\ \vdots & \ddots & \vdots \\ a_{31} & \cdots & a_{36} \end{pmatrix}. \tag{61}$$

The H_{inf} synthesis was performed in Matlab. Its hinfstruct() function successfully finds a stabilizing controller for all satellites and achieves closed-loop H_{inf} norm values of $\gamma = 0.679$ for satellites 1 to 4 and $\gamma = 0.641$ for satellite 5 after 305 iterations. For satellite 1 to 4 the stabilizing controller is computed to:

$$A_c = \begin{pmatrix} -0.347 & -1.382 & 0.882 & 0.889 & 0.841 & -0.173 \\ 0.262 & -1.505 & -0.644 & -0.813 & 0.073 & -0.090 \\ -0.710 & -0.258 & -0.731 & -0.673 & -0.678 & 1.062 \\ 0.207 & 0.957 & -0.102 & -1.703 & 0.740 & 0.189 \\ -0.138 & 0.606 & 0.329 & 0.226 & 0.018 & 0.235 \\ 1.481 & -0.038 & -0.962 & -0.225 & -0.459 & -1.700 \end{pmatrix} \tag{62}$$

$$B_c = \begin{pmatrix} -0.753 & -0.398 & -0.494 & -0.246 & 0.608 & 0.171 \\ -0.057 & 0.070 & -0.706 & 0.050 & 0.249 & -0.114 \\ 0.228 & -0.271 & -0.709 & -0.571 & 0.154 & -0.258 \\ -0.169 & 0.212 & 0.329 & 0.230 & -0.416 & -0.166 \\ 0.293 & 0.344 & 0.799 & 0.367 & 0.406 & -0.060 \\ -0.063 & -0.290 & -0.336 & -0.143 & -0.745 & 0.392 \end{pmatrix} \tag{63}$$

$$C_c = \begin{pmatrix} 0.198 & -0.396 & 0.492 & 0.202 & 0.695 & -0.477 \\ 0.123 & -0.184 & -1.057 & -1.942 & -0.107 & 0.469 \\ 0.265 & 1.011 & -0.315 & -0.669 & -0.112 & -0.075 \end{pmatrix} \tag{64}$$

$$D_c = \begin{pmatrix} -0.496 & 0.106 & -0.163 & 0.050 & -0.184 & 0.135 \\ 0.167 & 0.115 & -0.458 & -0.052 & -0.162 & -0.293 \\ 0.113 & 0.027 & 0.229 & -0.003 & -0.509 & -0.013 \end{pmatrix}. \tag{65}$$

The computed controllers for satellites 1 to 4 are identical, because their positions and connections within the network topology (as shown in Figure 11) are symmetric. Satellite 5 differs and thus the H_{inf} synthesis leads to a different controller:

$$A_c = \begin{pmatrix} -0.903 & -1.186 & -0.761 & 0.483 & 0.195 & -0.041 \\ -0.981 & -0.334 & 0.910 & 0.396 & -0.539 & -0.130 \\ -0.937 & -0.042 & 0.215 & -0.273 & -1.667 & -0.087 \\ 0.204 & 0.137 & -0.172 & 0.109 & 0.029 & -0.081 \\ 0.856 & 0.426 & -0.123 & -0.115 & 2.840 & 0.302 \\ -1.612 & -0.540 & 1.686 & 0.581 & -2.489 & -0.350 \end{pmatrix} \tag{66}$$

$$B_c = \begin{pmatrix} -0.903 & -1.186 & -0.761 & 0.483 & 0.196 & -0.041 \\ -0.981 & -0.334 & 0.910 & 0.396 & -0.539 & -0.130 \\ -0.937 & -0.042 & 0.215 & -0.273 & -1.667 & -0.087 \\ 0.204 & 0.137 & -0.172 & 0.109 & 0.029 & -0.081 \\ 0.858 & 0.426 & -0.123 & -0.115 & 2.840 & 0.302 \\ -1.612 & -0.540 & 1.686 & 0.581 & -2.489 & -0.351 \end{pmatrix} \tag{67}$$

$$C_c = \begin{pmatrix} 0.295 & -0.606 & -0.184 & -0.504 & 0.219 & 0.207 \\ -0.419 & 0.540 & -0.191 & -1.692 & 0.404 & -0.241 \\ 0.457 & 1.008 & 0.203 & 0.523 & -0.201 & -0.413 \end{pmatrix} \tag{68}$$

$$D_c = \begin{pmatrix} -0.461 & -0.048 & 0.201 & 0.091 & -0.364 & -0.076 \\ -0.055 & -0.175 & -0.597 & 0.040 & -0.259 & -0.067 \\ 0.285 & 0.260 & 0.168 & -0.084 & -0.439 & -0.040 \end{pmatrix}. \tag{69}$$

With these controllers, the given example can be simulated.

3.2. Simulation Results

The Hill's equations (Equation (2)) are used as the propagation model for the simulations performed. Although, they are limited in accuracy for specific applications (e.g., large scale formations, eccentric orbits) and do not include orbit perturbations (like J2 effect or atmospheric drag), they are suitable and sufficient for the considered scenario.

As target reference a static (in LVLH frame fixed and not moving) pentahedral formation as required for a spaceborne telescope is used. It shows a 10×10 m base in the x–y plane and the tip is located at -10 m along z axis. This target formation was not force-free, which means that orbit dynamics (cf. Equation (1)) were acting on the satellites and degrading the formation topology. Thus, after acquiring this formation, the controllers remain active for maintaining it. The satellites start from initial positions on v-bar $(-20, -10, 0, 10, 20$ m), which are—in contrast to the target formation—force-free. So the initial formation would not degrade due to orbit dynamics and active control is required to move the satellites away from it. Figures 12–15 show the trajectories of the five satellites from the given starting points to the pentahedral target formation. Figure 16 shows the control accelerations and disturbance acting on satellite 1.

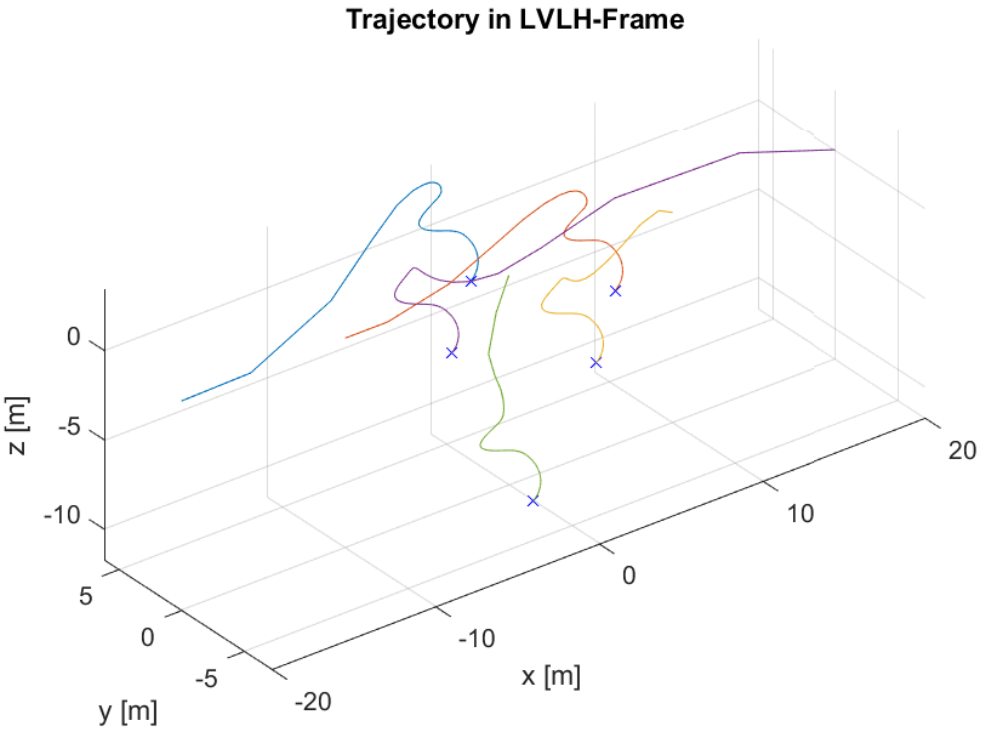

Figure 12. 3D plot of the trajectories of the five satellites subject to the presented consensus-based controller starting on v-bar $(-20, -10, 0, 10, 20$ m).

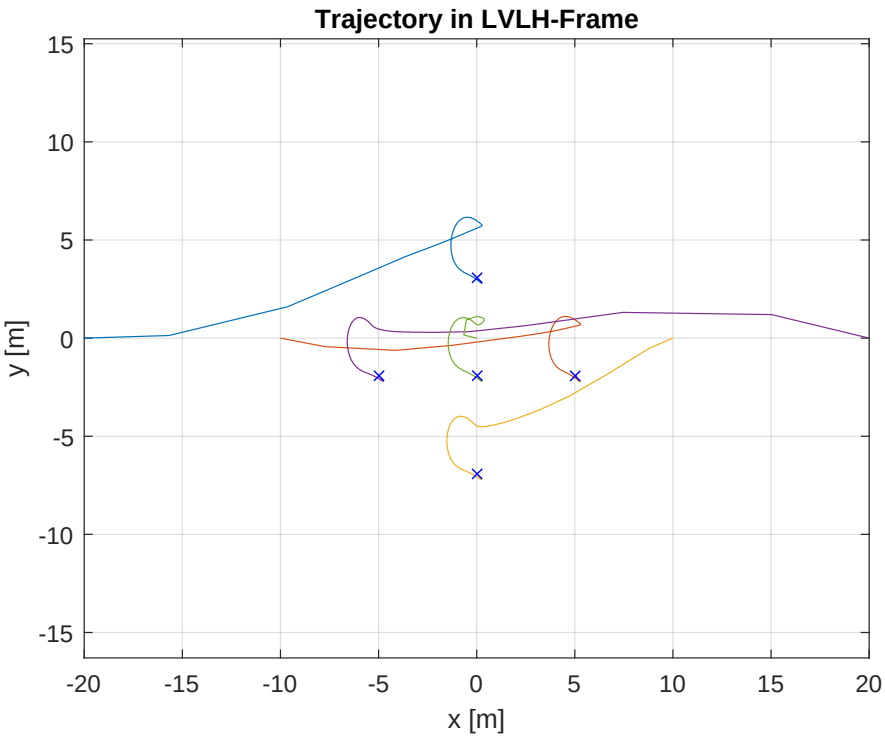

Figure 13. The x–y motion of the trajectories of the five satellites subject to the presented consensus-based controller starting on v-bar $(-20, -10, 0, 10, 20$ m).

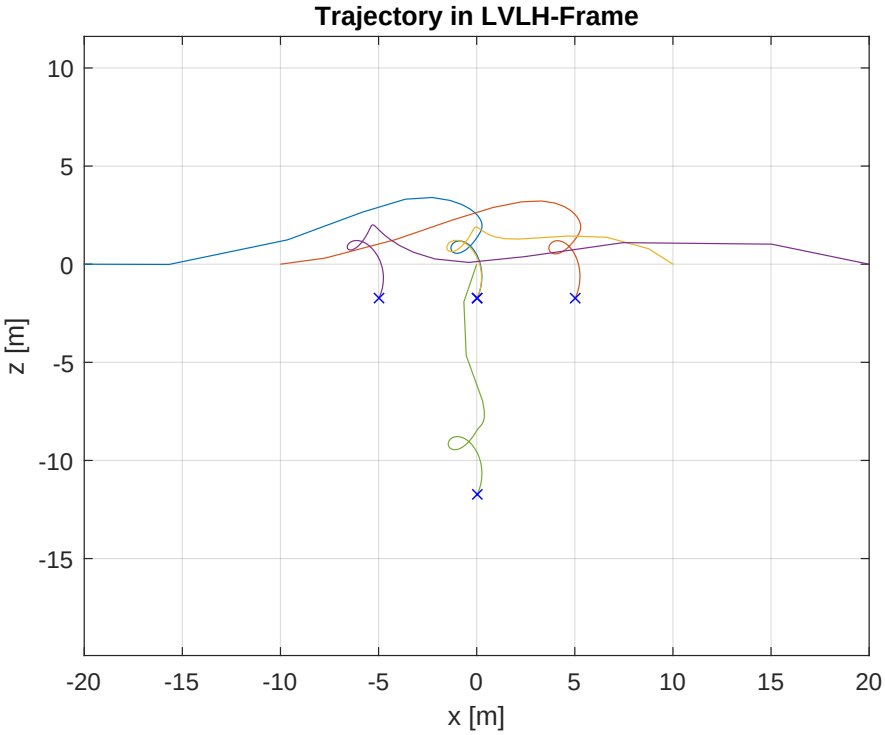

Figure 14. The x–z motion of the trajectories of the five satellites subject to the presented consensus-based controller starting on v-bar $(-20, -10, 0, 10, 20$ m).

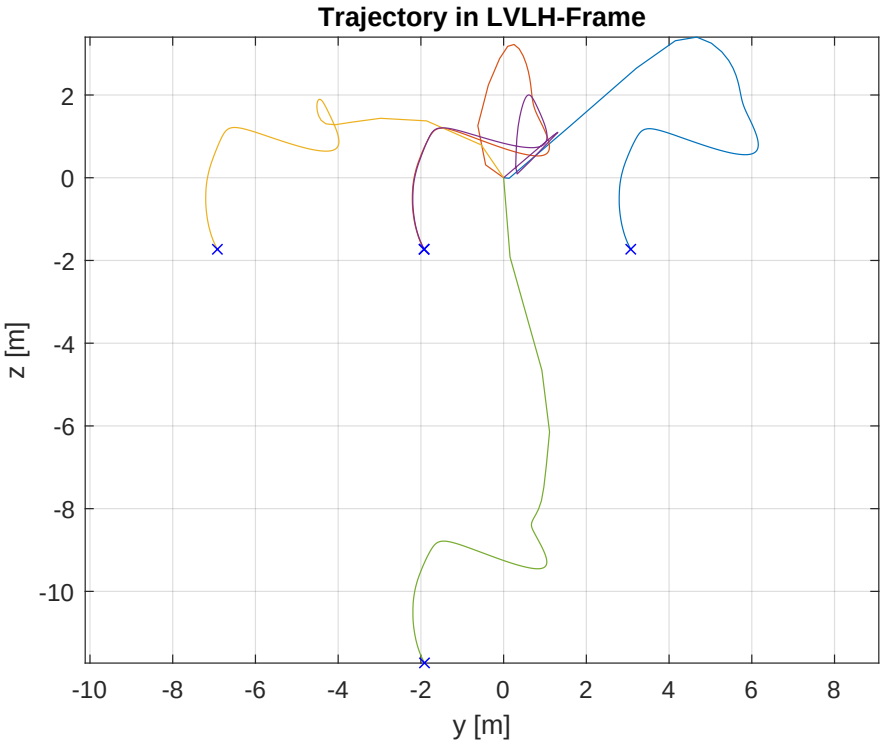

Figure 15. The y–z motion of the trajectories of the five satellites subject to the presented consensus-based controller starting on v-bar $(-20, -10, 0, 10, 20$ m).

From Figures 12–15 one can clearly see the convergence of the satellites' positions from their starting points towards the desired target formation. During this transfer the controller counteracts

both, the orbital dynamics given by the Hill's equations (Equation (1)) and the induced disturbances (thruster perturbations). Figure 16 shows the control effort required for this transfer. As one can clearly see, most control acceleration is applied during the first seconds of the maneuver, which is mainly applied for changing the satellites' position and converging to the target states. After that, the controllers remain active to force the satellites to stay on their target positions. The controllers are counteracting disturbances and—since the formations are not force-free—also orbit dynamics, which would cause a degradation of the formation. However, this formation maintenance requires much less control acceleration than the initial tracking.

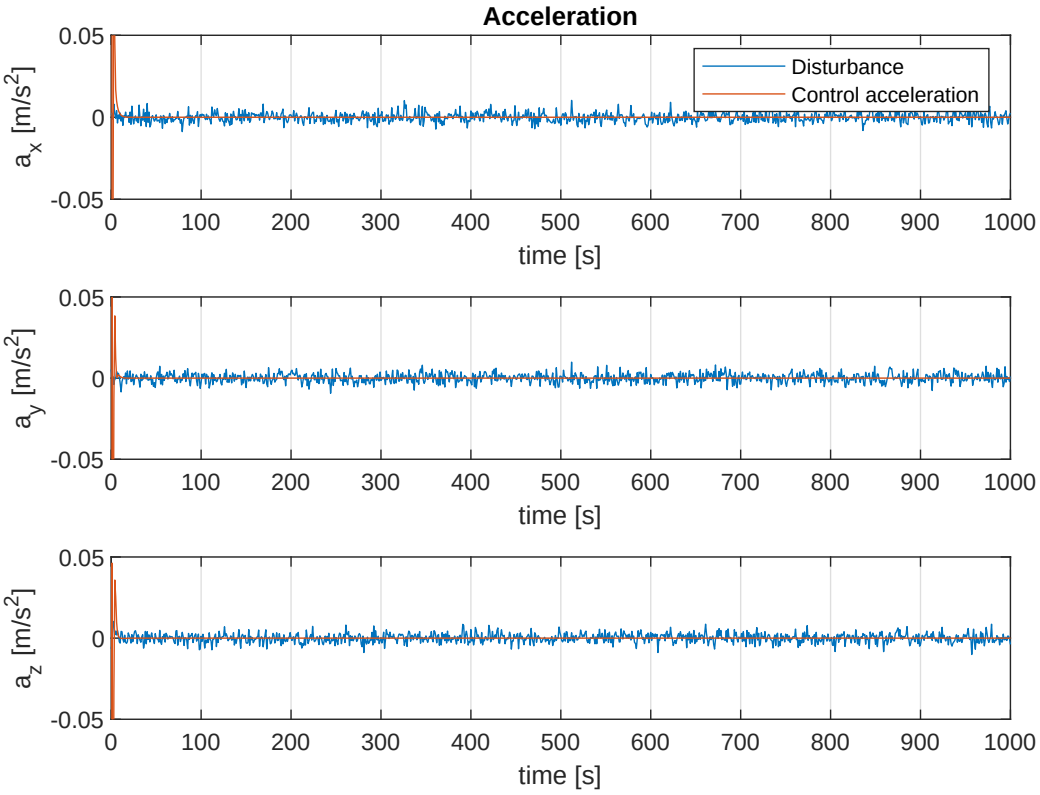

Figure 16. Accelerations acting on satellite 1 during simulation time, namely disturbance and control acceleration.

Fixing Coordinate Origin to an Agent

Following Section 2.4.6, it is also possible to fix one satellite (e.g., satellite 5) at the coordinate frame origin and let it be passive and uncontrolled with respect to reference tracking. This is done by adjusting the adjacency, degree and Laplacian matrices:

$$D_g = \begin{pmatrix} 3 & 0 & 0 & 0 & 0 \\ 0 & 3 & 0 & 0 & 0 \\ 0 & 0 & 3 & 0 & 0 \\ 0 & 0 & 0 & 3 & 0 \\ 0 & 0 & 0 & 0 & \mathbf{0} \end{pmatrix} \tag{70}$$

$$A_j = \begin{pmatrix} 0 & 1 & 0 & 1 & 1 \\ 1 & 0 & 1 & 0 & 1 \\ 0 & 1 & 0 & 1 & 1 \\ 1 & 0 & 1 & 0 & 1 \\ \mathbf{0} & \mathbf{0} & \mathbf{0} & \mathbf{0} & 0 \end{pmatrix} \tag{71}$$

$$L = D_g - A_j = \begin{pmatrix} 3 & -1 & 0 & -1 & -1 \\ -1 & 3 & -1 & 0 & -1 \\ 0 & -1 & 3 & -1 & -1 \\ -1 & 0 & -1 & 3 & -1 \\ \mathbf{0} & \mathbf{0} & \mathbf{0} & \mathbf{0} & \mathbf{0} \end{pmatrix}. \tag{72}$$

The controller for satellite 5 differs from the previous scenario, since its according part of the Laplacian matrix is different. Thus, the H_{inf} synthesis leads to a different stabilizing controller for satellite 5. After 310 iterations it achieves a closed-loop H_{inf} norm value of $\gamma = 1.07$. The controller in its state-space representation is given as:

$$A_c = \begin{pmatrix} -0.135 & -0.109 & 0.240 & 0.049 & 0.073 & 0.307 \\ 0.449 & -2.100 & 1.052 & -0.281 & -0.247 & 1.739 \\ 0.518 & 0.049 & -0.650 & -0.023 & 0.073 & -0.340 \\ -0.133 & 0.105 & 0.099 & -1.408 & 0.065 & -0.339 \\ 1.053 & 0.202 & -0.995 & 0.029 & -0.210 & -0.415 \\ 0.616 & -0.262 & -1.072 & 0.595 & -0.159 & -1.112 \end{pmatrix} \tag{73}$$

$$B_c = \begin{pmatrix} -0.049 & 0.164 & 0.257 & -0.154 & 1.975 & 0.449 \\ -0.388 & 0.854 & -1.063 & -0.901 & 1.391 & -0.138 \\ -0.569 & -0.275 & 0.705 & 0.127 & 1.668 & 0.578 \\ -0.068 & -0.161 & -0.772 & -0.326 & -0.277 & 0.038 \\ -0.166 & -0.118 & 0.751 & 0.237 & -0.680 & -1.239 \\ -1.178 & -0.719 & 0.870 & 0.742 & -1.779 & -0.189 \end{pmatrix} \tag{74}$$

$$C_c = \begin{pmatrix} 0.866 & 0.784 & -0.781 & 0.442 & 0.070 & 0.258 \\ 0.664 & 0.005 & -0.636 & 1.102 & -0.057 & 0.090 \\ -1.094 & 0.005 & 0.913 & 0.153 & 0.081 & 0.177 \end{pmatrix} \tag{75}$$

$$D_c = \begin{pmatrix} 0.843 & 0.094 & 0.104 & 0.038 & -0.181 & -0.058 \\ -0.090 & -0.027 & 0.815 & 0.345 & 0.098 & -0.012 \\ 0.183 & 0.177 & -0.041 & -0.053 & 0.806 & 0.301 \end{pmatrix}. \tag{76}$$

Even though one satellite is now not following any external target reference any more, the other satellites adjust their position to form the formation topology defined as reference. Figure 17 visualizes this behavior.

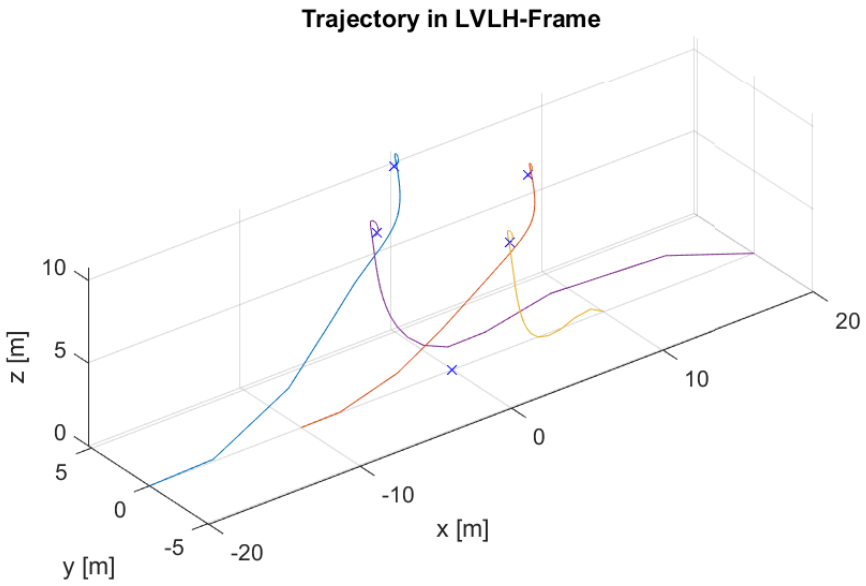

Figure 17. 3D plot of the trajectories of the five satellites subject to the presented robust consensus-based controller starting on v-bar $(-20, -10, 10, 20, 0$ m). One satellite is fixed at the origin and uncontrolled. Still, the other satellites adjust their states to form the desired formation.

4. Discussion

This paper presents a new approach of combining the fields of distributed control and robust control. The distributed consensus approach is related to classical H_∞ robust control. A generalized plant description including disturbances, noise and a formation topology as target reference has been derived for each single agent in a distributed setup. This plant description is suited to H_∞ synthesis, which can compute the distributed robust controller. In addition, a generalized plant description describing the overall system is presented as well.

Special focus was set towards space applications, namely satellite formation flying, both during controller design as well as during the simulations. Thus, as scenario a spaceborne distributed telescope has been used. It consists of a 3D formation. Both, convergence towards this formation as well as maintaining it, has been simulated. The simulation results are presented that show the applicability of the developed distributed robust control method to this simple, though realistic space scenario. By using this method, an arbitrary number of satellites/agents can be controlled towards any formation geometry. The developed combination with robust H_∞ control suffices the high stability and robustness demands of space applications. Of course, this control approach is applicable and beneficial for other application areas as well.

As future work continuing this development the simulations can be extended by adding realistic sensor noise in addition to the implemented disturbances. The simulation of additional scenarios would improve the evaluation of this control approach for further applications. A comparison with other control approaches suiting the presented scenario would help to assess the performance of the presented approach. Additionally, the implementation of collision avoidance would pave the way for a real-world application of this control approach and further broaden the field of possible applications. The implementation of physical constraints (e.g., maximum allowed thrust) would also further improve the presented approach towards real-world applications, since in many cases constraints are required. Last but not least, the implementation and demonstration of this controller in

a real-world application would finally prove its applicability. This is planned within the upcoming satellite formation flying mission NetSat.

Author Contributions: Conceptualization, J.S. and F.K.; formal analysis, J.S.; funding acquisition, K.S.; methodology, J.S.; project administration, J.S. and K.S.; software, J.S.; supervision, K.S.; validation, J.S. and F.K.; visualization, J.S.; writing—original draft, J.S. and F.K.

Funding: The research was funded by the European Research Council (ERC) within the Advanced Grant "NetSat" under the Grant Agreement No. 320377 and by the European Space Agency (ESA) by the Networking/Partnering Initiative (NPI) under Contract No. 4000113715/15/NL/MH/ats.

Conflicts of Interest: The authors declare no conflict of interest. The founding sponsors had no role in the writing of the manuscript, and in the decision to publish the results.

Abbreviations

The following abbreviations are used in this manuscript:

AILRC	adaptive iterative learning reliable control
ATV	automated transfer vehicle
CLTF	closed-loop transfer function
ESA	European Space Agency
ISS	International Space Station
LEO	low Earth orbit
LFT	linear fractional transformation
LQR	linear quadratic regulator
LTI	linear time-invariant
LVLH	local-vertical, local-horizontal
MMS	Magnetospheric Multiscale Mission
MPC	model predictive control
NASA	National Aeronautics and Space Administration
NetSat	networked pico-satellite distributed system control
PCO	projected circular orbit
SFF	satellite formation flying
TF	transfer function

References

1. Fox, K.C. *NASA's MMS Spacecraft Achieve Tightest Flying Formation Ever*; NASA's Goddard Space Flight Center: Greenbelt, MD, USA, 2015.
2. Bonin, G.; Roth, N.; Armitage, S.; Newman, J.; Risi, B.; Zee, R.E. CanX-4 and CanX-5 Precision Formation Flight: Mission Accomplished! In *Proceedings of the 29th Annual AIAA/USU Conference on Small Satellites*; AIAA: Logan, UT, USA, 2015.
3. Schilling, K.; Bangert, P.; Busch, S.; Dombrovski, S.; Freimann, A.; Kramer, A.; Nogueira, T.; Ris, D.; Scharnagl, J.; Tzschichholz, T. NetSat: A Four Pico/Nano-Satellite Mission for Demonstration of Autonomous Formation Flying. In Proceedings of the 66th International Astronautical Congress, Jerusalem, Israel, 12–16 October 2015.
4. Scharnagl, J.; Kremmydas, P.; Schilling, K. Model Predictive Control for Continuous Low Thrust Satellite Formation Flying. In *Proceedings of the IFAC Workshop on Networked & Autonomous Air & Space Systems*; IFAC: Santa Fe, NM, USA, 2018.
5. Steindorf, L.M.; Amico, S.D.; Scharnagl, J.; Kempf, F.; Schilling, K. Constrained Low-Thrust Satellite Formation-Flying Using Relative Orbit Elements. In *Proceedings of the 27th AAS/AIAA Space Flight Mechanics Meeting*; AAS: San Antonio, TX, USA, 2017.
6. Ankersen, F. Guidance, Navigation, Control and Relative Dynamics for Spacecraft Proximity Maneuvers. Ph.D. Thesis, Aalborg University, Aalborg, Denmark, 2010.
7. Franzini, G.; Innocenti, M. Nonlinear H-infinity control of relative motion in space via the state-dependent Riccati equations. In Proceedings of the 54th IEEE Conference on Decision and Control, Osaka, Japan, 15–18 December 2015; pp. 3409–3414.
8. Saska, M.; Mejía, J.S.; Stipanović, D.M.; Vonásek, V.; Schilling, K.; Přeučil, L. Control and navigation in manoeuvres of formations of unmanned mobile vehicles. *Eur. J. Control* **2013**, *19*, 157–171. [CrossRef]
9. Ji, H.; Hou, Z.; Fan, L.; Lewis, F.L. Adaptive iterative learning reliable control for a class of non-linearly parameterised systems with unknown state delays and input saturation. *IET Control Theory Appl.* **2016**, *10*, 2160–2174. [CrossRef]

10. Haidegger, T.; Kovács, L.; Precup, R.E.; Benyó, B.; Benyó, Z.; Preitl, S. Simulation and control for telerobots in space medicine. *Acta Astronaut.* **2012**, *81*, 390–402. [CrossRef]
11. Schilling, K. Networked Control of Cooperating Distributed Pico-Satellites. In *Proceedings of the 19h IFAC World Congress*; IFAC: Cape Town, South Africa, 2014; Volume 19, pp. 7960–7964.
12. Wie, B. *Space Vehicle Dynamics and Control*; AIAA Education Series; AIAA: Reston, VA, USA, 1998.
13. Ren, W.; Cao, Y. *Distributed Coordination of Multi-Agent Networks*; Springer: London, UK, 2011.
14. Scharf, D.P.; Hadaegh, F.Y.; Ploen, S.R. A Survey of Spacecraft Formation Flying Guidance and Control (Part I): Guidance. In *Proceedings of the 2003 American Control Conference*; IEEE: Denver, CO, USA, 2003; pp. 1733–1739.
15. Scharf, D.P.; Hadaegh, F.Y.; Ploen, S.R. A Survey of Spacecraft Formation Flying Guidance and Control (Part II): Control. In *Proceedings of the 2004 American Control Conference*; IEEE: Boston, MA, USA, 2004; pp. 2976–2985.
16. Massioni, P.; Keviczky, T.; Gill, E.; Verhaegen, M. A Decomposition-Based Approach to Linear Time-Periodic Distributed Control of Satellite Formations. *IEEE Trans. Control Syst. Technol.* **2011**, *19*, 481–492. [CrossRef]
17. Li, Z.; Duan, Z.; Xie, L.; Liu, X. Distributed Robust Control of Linear Multi-Agent Systems with Parameter Uncertainties. *Int. J. Control* **2012**, *85*, 1039–1050. [CrossRef]
18. Xue, D.; Gusrialdi, A.; Hirche, S. Robust Distributed Control Design for Interconnected Systems under Topology Uncertainty. In *2013 American Control Conference*; AACC: Washington DC, USA, 2013; pp. 6541–6546.
19. Amini, A.; Azarbahram, A.; Sojoodi, M. H_inf Consensus of nonlinear complex multi-agent systems using dynamic output feedback controller: An LMI approach. *arXiv* **2015**, arXiv:1501.04859.
20. Li, Z.; Chen, J. Robust Consensus of Linear Feedback Protocols over Uncertain Network Graphs. *IEEE Trans. Autom.Control* **2017**, *62*, 4251–4258. [CrossRef]
21. Space Station Control Board. *SSP 30219 Revision J—Space Station Reference Coordinate Systems*; Technical Report; NASA, ESA, JAXA, CSA, ASI, RSA: Houston, TX, USA, 2008.
22. Hill, G. Researches in the Lunar Theory. *Am. J. Math.* **1878**, *1*, 245–260. [CrossRef]
23. Fehse, W. *Automated Rendezvous and Docking of Spacecraft*; Cambridge Aerospace Series; Cambridge University Press: Cambridge, UK, 2003.
24. Tian, Y.P. *Frequency-Domain Analysis and Design of Distributed Control Systems*, 1st ed.; Wiley: Singapore, 2012; p. 271.
25. Lunze, J. *Regelungstechnik 1: Systemtheoretische Grundlagen, Analyse und Entwurf Einschleifiger Regelungen*, 10th ed.; Springer: Heidelberg, Germany, 2014; p. 744.
26. Robert, C.P.; Marin, J.M.; Rousseau, J. Distributed Consensus in Multi-Vehicle Cooperative Control: Theory and Applications (Ren, W. and Beard, R.W.; 2008) [Book Shelf]. *IEEE Control Syst.* **2010**, *30*, 85–86,
27. Zhou, K.; Doyle, J.C.; Glover, K. *Robust and Optimal Control*; Prentice Hall: Englewood Cliffs, NJ, USA, 1996.
28. Lunze, J. *Regelungstechnik 2: Mehrgrößensysteme, Digitale Regelung*, 8th ed.; Springer: Berlin, Germany, 2014; p. 696.
29. Skogestad, S.; Postlethwaite, I. *Multivariable Feedback Control: Analysis and Design*, 2nd ed.; Wiley: Chichester, UK, 2001.
30. Doyle, J.; Packard, A.; Zhou, K. Review of LFTs, LMIs, and mu. In *Proceedings of the 30th IEEE Conference on Decision and Control*; IEEE: Brighton, UK, 1991; pp. 1227–1232.